2007

Detection of trace Al in model biological tissue with laser-induced breakdown spectroscopy

M.D. Adamson

Steven J. Rehse
University of Windsor

Detection of trace Al in model biological tissue with laser-induced breakdown spectroscopy

Marian D. Adamson and Steven J. Rehse*

Department of Physics and Astronomy, Wayne State University, Detroit, Michigan 48201, USA

*Corresponding author: rehse@wayne.edu

Received 12 January 2007; revised 30 March 2007; accepted 29 May 2007;
posted 20 June 2007 (Doc. ID 78984); published 9 August 2007

Laser-induced breakdown spectroscopy (LIBS), which is an excellent tool for trace elemental analysis, was studied as a method of detecting sub-part-per-10^6 (ppm) concentrations of aluminum in surrogates of human tissue. Tissue was modeled using a 2% agarose gelatin doped with an Al_2O_3 nanoparticle suspension. A calibration curve created with standard reference samples of known Al concentrations was used to determine the limit of detection, which was less than 1 ppm. Rates of false negative and false positive detection results for a much more realistic sampling methodology were also studied, suggesting that LIBS could be a candidate for the real-time *in vivo* detection of metal contamination in human soft tissue.

OCIS codes: 120.1880, 140.3440, 170.1020, 170.6510, 300.6210, 300.6360.

1. Introduction

Research is currently being performed within Wayne State University's Smart Sensors and Integrated Microsystems (SSIM) program to study the development of electronic implants for the eyes, spinal cord, and brain. Such biocompatible neurological implants offer real hope to people who are experiencing the debilitating effects of Parkinson's disease, macular degeneration, and a host of other medical conditions [1]. Such devices are designed to reroute brain-to-body connections around disease-ravaged or accident-damaged areas, and therefore at least partially restore muscle movement, vision, and other normal functioning.

One proposed technique to restore some form of vision to persons lacking sight is to implant a microfabricated chip into the retina to generate electrical impulses that send a sight pattern to the brain [2–5]. Such sensors embedded for lengths of time in human tissue should be chemically inert and should not react negatively with any biological tissue or process. This is the common requirement of "biocompatibility." For this reason, sapphire, Al_2O_3, which has good optical qualities as well as being hard and inert, is often used. However, there are concerns that the Al in these sapphire substrate retinal implants may tend to diffuse or leach into the surrounding tissue due to the chemical potential mismatch between substrate and tissue. Such a deposition of Al into retinal tissue could cause adverse performance of the implant and would also deposit harmful metals into the tissue [6].

In this paper, laser-induced breakdown spectroscopy (LIBS) has been studied as a diagnostic technique to accurately assess trace Al concentrations in simulated soft biological tissues. The inherent advantages of LIBS, such as speed, accuracy, relatively minimal sample destructiveness (small sampling areas), and a high spatial resolution on the target surface, all lend themselves to an analysis that could be utilized (potentially *in vivo*) to assess metal concentrations in tissues in which implants had been placed. The use of LIBS for the analysis of soft tissue has been described previously for the characterization of malignant cells [7] and on calcified tissues for the measurement of important minerals and potentially toxic elements (such as Al, Pb, and Sr) [8]. In fact, LIBS is particularly well-suited for the detection and quantification of trace metal contaminants that are toxic or harmful to humans (such as arsenic or mercury) with typical limits of detection (LOD) in the 10 parts per 10^9 (ppb) to 10 parts per 10^6 (ppm) range [9].

0003-6935/07/235844-09$15.00/0

We have utilized the LIBS technique to determine the LOD of nanoparticle-sized Al in simulated biological tissue both with and without a matrix emission line used for shot-noise "normalization." In both cases a sub-ppm LOD was measured. We have also investigated the use of a realistic sampling methodology (one or two laser sampling locations on the target) as a test of the applicability of the technique to actual clinical analysis where the available tissue area may be quite small and residual damage must be avoided. We present the advantages gained by using as little as two sampling locations on the target as compared to a single sampling location. Finally, the results of these low sampling number tests are presented as a function of the sensitivity and specificity of the test, a measurement of the rates of false positives and false negatives. The construction of a receiver operating characteristic (ROC) curve from these results provided a figure of merit for the technique that indicates its potential usefulness as a clinical diagnostic test.

2. Experiment

A. Model Tissue Preparation

Model biological tissue samples were fabricated to simulate real human tissue for all LIBS testing. This was done due to the ease with which such samples could be produced, the superiority of sample reproducibility and uniformity afforded by the model tissues, and the ability to prepare standard contaminated samples with precisely known concentrations of trace elements. An electrophoresis grade agarose (Fisher Chemical, BP161-100) gelatin was used to simulate human soft tissue (particularly located around the eyes), which is largely water and contains the elements C, H, N, and O [10]. The agarose gelatin also contained these elements, as well as Na and Ca, which are also likely to be contained in any human tissue. Agarose is commonly used in the field of medical physics as a magnetic resonance imaging (MRI) phantom equivalent to human tissues, as are gelatin, carrageenan, and agar, due to its very similar chemical composition and its physical/structural characteristics [11–13].

We created 100 g samples of 2% agarose gelatin with ultrapure water in flat-bottomed Petri dishes with an 8 cm diameter. The top surfaces of the agarose gelatins formed in this way were subject to curvature, bubbles, and other irregularities during the solidification process. Therefore, samples were cut out of the dish and carefully turned over to expose the very flat-bottom side for LIBS measurements.

Precisely measured amounts of Al were added to the agarose gelatins during the liquid stage of their fabrication to create a library of standard concentration samples with concentrations ranging from 10 to 1140 ppm. Known masses of a 20% Al_2O_3 nanoparticle/water colloidal dispersion (Alfa Aesar, 12733) with 50 nm particles were added and thoroughly mixed in with the agarose prior to solidification to distribute uniformly the nanoparticles throughout the agarose samples. The Al_2O_3 nanoparticles remained indefinitely in suspension even in water, ensuring there was no settling out of Al in the samples. No evidence of aluminum inhomogeneity on large length scales was observed in the model tissues created and doped in this way. Additionally, the models proved to be quite robust, lasting many days with minimal dehydration and no surface degradation if kept covered.

B. LIBS

The system used to perform LIBS on the tissue models is shown schematically in Fig. 1. An Nd:YAG laser (Spectra-Physics, LAB-150-10) was used at its fundamental frequency of 1064 nm. Pulses of 10 ns duration were produced with typical pulse energies of 80 mJ/pulse. Pulse energy attenuation was accomplished with a half-wave plate and a Glan laser polarizer. The Nd:YAG laser was capable of operation at a 10 Hz repetition frequency, but typical experiments utilized only three sequential pulses, followed by a delay of approximately 4 s, during which the sample was translated to provide a fresh target surface.

The laser pulses were focused onto the surface of the model tissues with two crossed-axis cylindrical lenses. Primary focusing was accomplished by an antireflection (AR)-coated $f = 40$ mm cylindrical lens that focused the ablation pulses to a line approximately 100 μm in width. The line-focused laser beam sampled a much larger target area per pulse and provided a significant improvement in spectrum reproducibility over a 5× microscope objective and conventional spherical lens [14]. The second cylindrical lens (AR coated, $f = 75.6$ mm) was placed in front of the focusing lens with its axis rotated perpendicular to the focusing lens's axis. This second lens was translated to control the length of the focused ablation line and thus the total energy density in the ablation spot. The resulting ablation line was an ellipse approximately 1 mm × 100 μm.

The model tissues were mounted on a three-axis translation stage for alignment and translation during ablation. Typically the model tissue was manu-

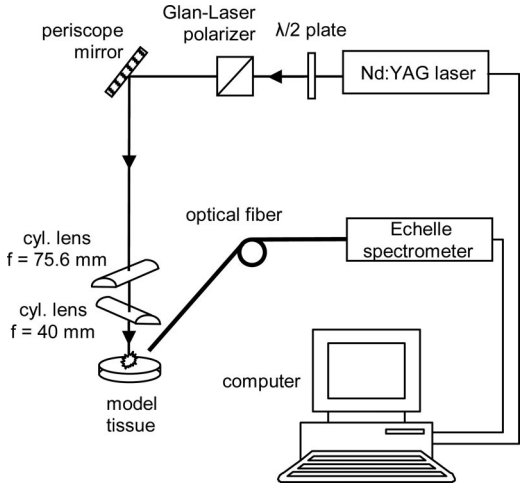

Fig. 1. Experimental diagram of the LIBS apparatus used in this study.

ally translated by 635 μm (0.025 in.) between sets of three laser pulses. Reproducibly setting the distance from the focusing cylindrical lens to the sample was extremely important, as a variation of only 0.25 mm was found to change noticeably the resulting LIBS spectrum. Therefore an 80 pitch screw attached to the lens holder was used as an adjustable guide to assist in obtaining accurate and reproducible sample/lens spacing.

Light was collected via a 1 m steel encased multimode optical fiber (core diameter = 600 μm, N.A. = 0.22) placed a distance of 23 mm from the ablation spot with no other light collection optics. Fiber alignment was achieved by coupling a HeNe laser into the opposite end of the fiber and allowing the resulting cone of light from the sample end to overlap the area of ablation. The output end of the fiber was coupled to an echelle spectrometer (LLA Instruments GmbH, ESA 2000). The echelle spectrometer utilized a 1024 × 1024 CCD-array (24 μm^2 pixel area) with an image intensifier (ICCD) and was controlled by a PC running manufacturer-provided software. The PC controlled not only the gating (shuttering) of the ICCD, but also controlled operation of the pulsed laser via an onboard fast pulse generator to eliminate jitter in the time between laser pulse and plasma observation. The useful spectral range of the spectrometer was 200–834 nm with a 0.005 nm resolution in the UV.

To achieve the highest signal-to-noise ratio, the LIBS spectra from three individual 80 mJ laser pulses were accumulated on the CCD camera chip prior to readout. These on-chip accumulations (OCA) allowed a rapid averaging of the emission spectra, provided the resulting intensity did not exceed the dynamic response of the CCD chip. The sample was then translated 635 μm, another three ablation pulses fired, and the resulting spectrum was averaged in software with the previous three-pulse accumulation. Forty accumulations of three laser pulses (120 laser pulses total) were averaged together to form one "measurement." Typically, ten measurements (1200 laser pulses total) were made on each sample. The scatter in the results from the ten measurements allowed us to calculate a 1σ standard deviation uncertainty for our results. All spectra were obtained at a gate delay time (τ_d, the time between firing of the ablation pulse and electronic activation of the CCD camera's image intensifier) of 6 μs with a gate width (τ_w, integration time) of 20 μs. These values were chosen to maximize the signal-to-noise and signal-to-background of the observed Al emission and were not varied during the experiment.

3. Results and Discussion

A. LIBS Spectrum of Al-Doped Tissue Models

Figure 2 shows a typical LIBS spectrum from a 60 ppm Al-doped agarose model tissue ablated with a laser energy of 80 mJ/pulse and consisting of 38 accumulations of three laser pulses. Figure 2(a) shows the entire optical range that can be seen by the spectrometer, 200–834 nm. The most obvious atomic emission lines (Na, C, O, H, and Al) are labeled as are the dominant molecular emissions (NH and OH). The observation of strong molecular NH and OH bands was expected due to the high water content of the agarose sample (which is 98% water) and has been investigated by us in a previous work [15]. Figure 2(b) shows a detailed portion of the spectrum from 393.0 to 397.25 nm containing the Al I resonance lines and the Ca II emission lines utilized in this study. Although both Al lines are clearly visible, the stronger line at 396.152 nm was used for all analysis. No self-reversal of either Al emission line was observed at any concentration. The Ca II line used as a normalization reference line is shown on the left at 393.366 nm. Ca is a trace component of electrophoresis grade agarose, and its exact concentration in the agarose medium was undetermined by the manufacturer. However, all Al-doped samples were prepared from the same batch of agarose medium; therefore it is expected that the Ca concentration was constant across all samples.

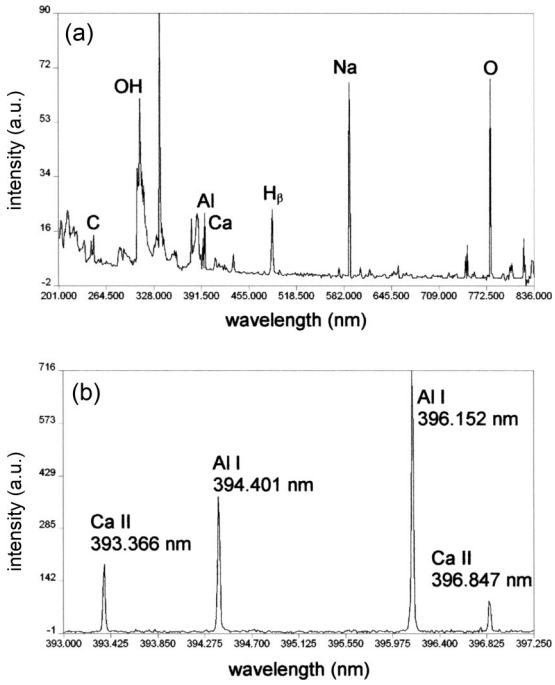

Fig. 2. Typical LIBS spectrum of a 60 ppm Al-doped agarose model tissue. LIBS parameters were τ_d = 6 μs, τ_w = 20 μs, 80 mJ/pulse, 38 accumulations of three OCA. (a) Broadband optical spectrum, 200–834 nm. (b) Closeup of the region of the spectrum containing the Al and Ca emission lines used in this study.

B. Concentration Curves

The intensity of both the Al 396 nm and Ca 393 emission lines shown in Fig. 2 was obtained by nonlinear least-squares fitting of the peaks to obtain the area under the line profile. The spectrometer software that controlled both the laser Q switching and the spectrometer timing (LLA Instruments GmbH, ESAWIN) also performed real-time curve-fitting of the emission lines utilizing a Lorentzian line shape to construct

calibration curves. This curve-fitting method was compared to a more manual method using a FORTRAN program that performed a numerical integration of the line profile, and complete agreement was found between the two.

Calibration curves plotting both the normalized Al/Ca emission intensity and the absolute Al emission intensity as a function of the varying Al concentration (from 10 to 1140 ppm) in nine model tissues were constructed from the standard samples and are shown in Fig. 3. While it is understood that it is generally prudent and advisable in LIBS to normalize the intensity of the analyte line to another matrix line due to random variations in plasma intensity caused by laser pulse energy fluctuations, nonuniformities in the sample, or sample placement, it may not always be feasible or practical. In particular, concentrations of Ca in real tissues from different specimens could be quite different. Therefore, a calibration curve was constructed for both the normalized Al line and the unnormalized line. Figure 3(a) shows the ratio of the Al line at 396 nm to the Ca line at 393 nm, while Fig. 3(b) shows the intensity of just the Al line at 396 nm in arbitrary units (a.u.). Each measurement of 40 accumulations is shown as an "x" in Fig. 3. The solid dot is the average of the ten measurements with the error bar determined by the standard deviation of the ten individual measurements. A weighted linear fit was performed on the average values to obtain the linear calibration curve, with the standard deviation of the ten measurements providing the weighting factor. The linear fit to the data in Fig. 3(a) provided χ^2 per degree of freedom of 2.17 compared to χ^2 per degree of freedom of 5.54 for the fit in Fig. 3(b). However, the fitting in both Figs. 3(a) and 3(b) produced a coefficient of determination (R^2) of 0.90. The linear fit was not constrained to pass through the origin in either graph.

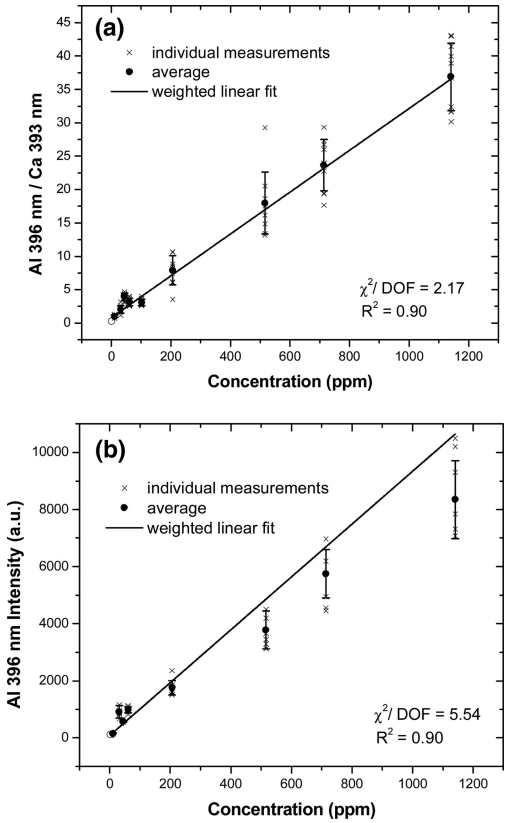

Fig. 3. LOD calibration curves showing emission intensity versus sample concentration. Lines are weighted linear fits to the data obtained from nine Al-doped 2% agarose model tissues. The fits are not constrained to pass through the origin. (a) Emission intensity of the Al 396 nm line has been normalized by the Ca 393 nm line. (b) Emission intensity of the Al 396 nm line has not been normalized. In both graphs, data from a 2 ppm sample (not included in the construction of the linear fit) are shown as an open circle.

Although it appears that the unnormalized data are beginning to show evidence of Al saturation, the quality of the linear fit is comparable to the normalized data and the calculated limit of detection (discussed below) is almost identical. The possibility of saturation at higher concentrations was investigated by constructing a fit composed of two linear segments, to allow for a change in slope at lower and higher concentrations. No evidence was found for a change in slope at higher concentrations, and it was highly unlikely that saturation was occurring at low concentration (e.g., under 100 ppm), as other studies of trace elements in varying matrices typically have shown much higher saturation regions or none at all [16,17]. Therefore, it was decided that the system demonstrated a linear relationship between 10 and 1140 ppm, and any slight deviation from linearity in slope at low or high concentrations were simply due to nonuniformities between samples. To test this, the normalized and unnormalized data from a 2 ppm sample are shown in Figs. 3(a) and 3(b) as an open circle. This data point was not included in the construction of the linear fit but clearly falls along the calibration line in both Figs. 3(a) and 3(b).

A study of the Ca II normalization line at 393 nm was also conducted to ensure that the intensity of this reference line was truly constant and independent of Al concentration. The intensity was constant within the uncertainty of any one measurement (~15% fractional uncertainty) with the exception of one sample of 100 ppm Al concentration that had accidentally been left uncovered and had experienced significant dehydration. An attempt was made to rehydrate the sample prior to testing with LIBS, yet after rehydration the sample retained a Ca intensity approximately six times greater than all other samples. However, a careful examination of Fig. 3(a) shows no deviation of the point corresponding to the 100 ppm sample from the fitted curve, indicating the effectiveness of the normalization technique. This point was not included in Fig. 3(b) due to its deviation from the unnormalized data trend. The behavior of this particular sample also implied that the scatter in the lower concentration region of the calibration curve could likely be due to small differences in sample hydration, which was not carefully controlled.

C. Limit of Detection

The LOD is the lowest concentration at which, ideally, an analyte signal can be discriminated from noise. The common definition in spectroscopy for the minimum value of a signal is 3σ [18], making the definition for the calculated limit of detection LOD $= 3\sigma/s$, where σ is the average noise of the background, and s is the slope of the calibration curve. The error on the LOD is calculated in the standard way by adding the fractional error of the slope and σ in quadrature, $\Delta\mathrm{LOD}/\mathrm{LOD} = \sqrt{(\Delta\sigma/\sigma)^2 + (\Delta s/s)^2}$.

Minimization of the LOD can be achieved by reducing the noise of the spectrum's background. Figure 4 shows the effect of increasing the delay time of observation [Fig. 4(a)] and laser pulse energy [Fig. 4(b)] on the noise in the background, σ. Figure 4(a) clearly shows that increasing the delay time before observing the LIBS plasma resulted in a significant reduction in noise. It is possible that this graph implies that increasing the delay time even more would be advantageous; however, a corresponding decrease in signal intensity then made accurate determination of the Al emission intensity difficult. A delay time of 6 μs was chosen as a compromise. Figure 4(a) also shows that at 6 μs or longer delay times, 20 accumulations achieved the same level of noise as 40 accumulations. The corresponding decrease in Al emission intensity, however, precluded this reduction of the number of accumulations. The increase in background noise as a function of increasing laser pulse energy shown in Fig. 4(b) clearly demonstrates that these LIBS measurements should be taken with as low a pulse energy as possible. Decreasing the pulse energy below 80 mJ degraded the Al signal too much to be effective.

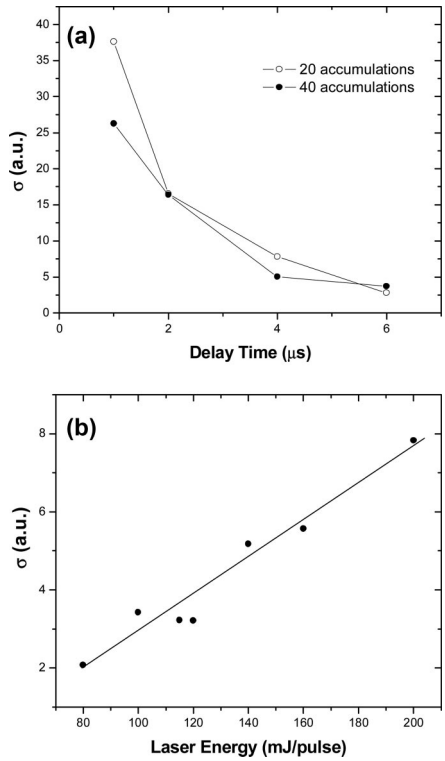

Fig. 4. Effect of (a) delay time and (b) laser energy on the noise of the background, σ, of the LIBS measurements. (a) Delay time study was performed with a laser energy of 120 mJ/pulse. (b) Pulse energy study was performed at a delay time of 6 μs.

Table 1. Al LOD in Model Tissue

	Calibration Curve Slope s	Background Noise σ	LOD (ppm)
Al/Ca	0.0313 ± 0.0028	0.0103 ± 0.0044	0.99 ± 0.43
Al	9.2545 ± 0.5415	2.5438 ± 0.0961	0.82 ± 0.09

The LODs calculated from the calibration curves in Fig. 3 are presented in Table 1. The limits calculated from both curves are just under 1 ppm and the unnormalized Al LOD falls within the error bars of the Al/Ca LOD. Although the uncertainly of the unnormalized LOD appears to be smaller, it is believed that the normalization provided a more reproducible emission intensity, and thus the normalized calibration curve offers an intrinsically more reliable and accurate determination of the LOD. To test the accuracy of these LOD measurements, a model tissue sample with an Al doping of 2 ppm was fabricated. The data from this sample were included in Fig. 3 as open circles but were not used in the construction of the linear fit. A 2 ppm sample was the lowest doping concentration that could be fabricated conveniently, reliably, and accurately given the method utilized to make these standard samples. LIBS analysis of this sample showed a very clear Al emission signal well over the 3σ limit for detection, proving that signals from samples with these low concentrations could be easily observed.

D. Few Accumulation Measurements

The Al limit of detection presented in Subsection 3.C was calculated from data points obtained by combining 10 measurements of 40 accumulations, each accumulation consisting of three laser pulses. The sample was translated between each accumulation. Each such set of measurements on the model tissue comprised an area approximately 25 mm × 20 mm. This is a fairly unrealistic testing methodology for a potential *in vivo* application or even *ex vivo* testing on tiny tissue samples. Therefore we investigated the ability to detect trace Al using only one, two, three, or four accumulations.

Al doped samples were prepared with concentrations of 100, 10, 2, and 0 ppm, and 40 individual LIBS spectra per concentration were acquired with a single accumulation using a laser energy of 80 mJ/pulse. Measurements of two, three, and four accumulations were acquired by averaging the spectra from consecutive single accumulations. The objective of this study was to determine what criterion should be utilized to indicate a successful or positive detection of Al and to then identify the percentage of accumulations that detected Al for each concentration (a true positive result) or failed to detect Al when it should

have (a false negative result). The 0 ppm sample was used to determine the number of false positives or times when Al was apparently detected (due to noise) when it should not have been. This type of testing could not return information on the actual Al concentration in the sample, the data being too noisy to use the results on the calibration curve constructed earlier, but could only detect the presence or absence of Al in a sample.

Due to the very low amount of spectral averaging performed, Al emission peaks within these spectra were much smaller and extremely noisy. Curve fitting for the determination of intensity was rejected and replaced with a simple MATLAB algorithm to average the three pixels (channels) of the ICCD around the Al emission peak. These consisted of the pixel centered on the emission wavelength and the two nearest-neighbor side pixels. To determine the background noise, a region of empty spectrum near the Al 396 nm emission line was binned and averaged into sets of three adjacent pixels as well. This binning of pixels exploited the fact that a true emission feature was spread over multiple pixels, but a noise spike was identifiable due to its consisting of only a single pixel. A standard deviation of the background was calculated from the newly averaged or smoothed region to define the noise or scatter of the spectrum. A positive detection of Al was then indicated when the average of the three Al pixels exceeded the background by an amount equal to some multiple of the noise of the background. The Al emission line was considered by itself, with no Ca normalization being performed.

Figure 5 shows the percentage of true positive Al detections "yes, Al was detected" and false negatives "no, Al was not detected" when Al-doped samples with three concentrations (2, 10, and 100 ppm) were measured with a single accumulation. The rates of false negatives can be seen in the undoped sample with 0 ppm Al. All "yes" detections on this blank sample constituted a false positive. The percentage of false positives was used as an error bar on the other data. The data were analyzed utilizing three different cutoff detection criteria: Al signals greater than 1σ, 3σ, or 10σ. In Fig. 5(a) it can be seen that using a 1σ cutoff is a very sensitive test, returning a high rate of detections for almost all concentrations, with concentrations of 10 and 100 ppm being detected almost 100% of the time. As expected, however, this test also yielded the highest rates of false positives, with Al being detected nearly 21% of the time in the blank sample. This is the reason for the large error bars in Fig. 5(a). This would be an appropriate testing criterion for lightly contaminated tissues and in situations where it would be more detrimental not to detect Al than to detect a false positive. Figure 5(b) shows the more sensible 3σ cutoff criterion. Using this cutoff, Al was still detected in 100 ppm samples 100% of the time and the 10 ppm sample 90% of the time. The detection efficiency (commonly called the sensitivity) decreased in the 2 ppm sample to only 55%, but the rate of false positives in the blank sample dropped to under 10%. The 10σ cutoff criterion

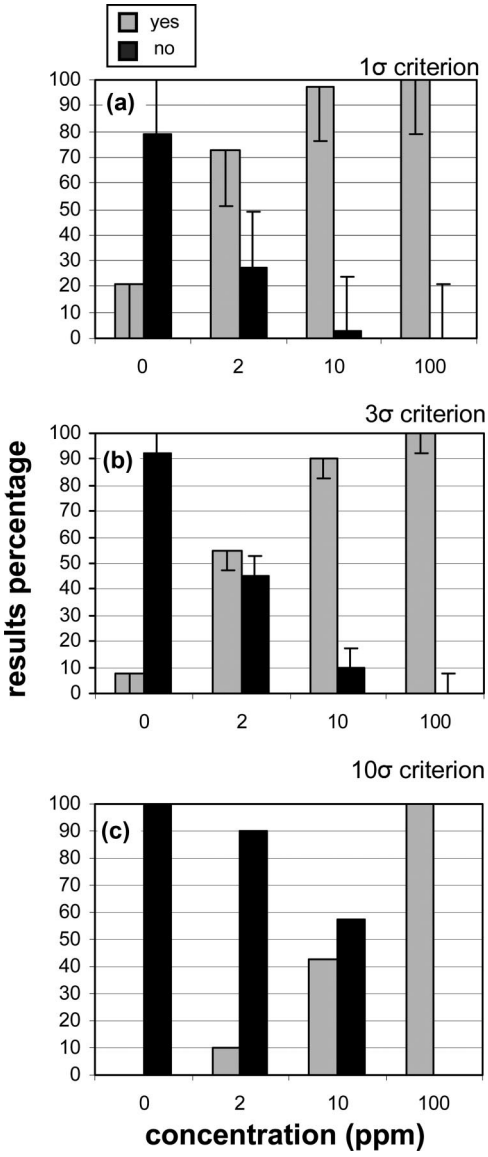

Fig. 5. Percentage of yes and no results from 40 single accumulation measurements on Al-doped model tissues with different concentrations. A yes result indicates the test was positive for Al. A no result indicates the test was negative for Al. (a) A 1σ criterion was used as the cutoff for detecting Al. (b) A 3σ criterion was used as the cutoff for detecting Al. (c) A 10σ criterion was used as the cutoff for detecting Al.

was the least sensitive, but had the highest specificity, retuning no false positives in all of the 40 tests. Al was still detected in the 100 ppm sample 100% of the time, but the ability to detect Al in the 2 ppm sample dropped to only 10%. This would be the appropriate testing criterion for a more heavily contaminated tissue.

Figure 6 shows the change in the sensitivity and specificity utilizing the 3σ criterion when more than one accumulation was used to sample different locations on the target surface. All tests used 80 mJ/pulse and were performed on the 2 ppm model tissue [Fig. 6(a)] and the blank 0 ppm model tissue [Fig. 6(b)]. It

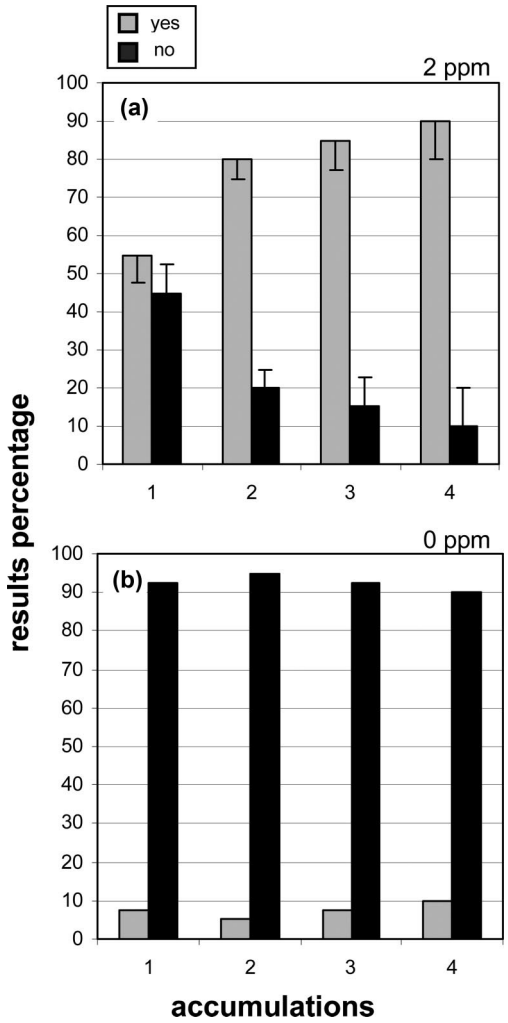

Fig. 6. (a) Percentage of yes and no results from 40 measurements on 2 ppm Al-doped model tissue utilizing either one, two, three, or four accumulations to make the measurement. (b) Percentage of yes and no results from 40 measurements on a blank, 0 ppm sample.

is clear from Fig. 6(a) that taking even one additional accumulation was beneficial, increasing the sensitivity of the result from 55% to 80%. Above two accumulations the increase was less substantial, but still evident, rising to a sensitivity of 90% for four accumulations. Figure 6(b) shows that the specificity was constant as a function of the number of accumulations, with each test returning a false negative result approximately 7% of the time.

It is important to note that Figs. 5 and 6 do not measure or indicate which cutoff criterion is best or how many accumulations should be optimally utilized. The decision of which criterion to use depends solely on the situation. For example, in a medical application, a false negative means a problem is not diagnosed. If the risk of falling ill due to the presence of the contaminant exceeds the harm caused by further testing, a 1σ test (the most sensitive) should be used to catch all possibilities that would merit further testing. However, if heavy contamination is expected, and missing trace amounts is noncritical, a 10σ test would be more appropriate. Also, the acquisition of more accumulations seems to be beneficial, but only if the target area available for testing is large and multiple laser pulses will not be detrimental to the tissue.

In this type of clinical diagnostic test, it is typical to plot the sensitivity (the true positive rate) on the y axis against the false positive rate (which is 1 specificity) on the x axis for all the different possible cutoff values of the test. This type of graph is called a ROC curve. Presented in this way, the curve itself becomes the relative figure of merit, with the area under the curve establishing the quality of the test as a statistical indicator of testing accuracy [19].

Figure 7 shows the ROC curve for 80 mJ/pulse LIBS obtained by systematically changing the noise cutoff criterion of the test. For any particular noise cutoff criterion, the results of testing the 0 ppm sample provided the specificity (the x-axis coordinate) and the results of testing the 2 ppm Al-doped model tissue provided the sensitivity (the y-axis coordinate). This was done for both one and two accumulations to show the improvement of the method when at least two accumulations were utilized. In this graph, the rate of false positives increases to the right as the noise cutoff of the test was decreased. At the origin, the cutoff for Al detection was 15σ, which returned no false positives (specificity = 1, or 1-specificity = 0) but also detected no Al (sensitivity = 0). As the cutoff was lowered the sensitivity and 1-specificity both increased, but not in the same way for the different number of accumulations. The 2 ppm data in Fig. 5 also shows this trend for one accumulation: with a 10σ cutoff the sensitivity was 10%, and with a 1σ cutoff the sensitivity was 72%. In Fig. 7, the cutoff was lowered to approximately -1σ for 1 accumulation and -0.3σ for two accumulations to reach a sen-

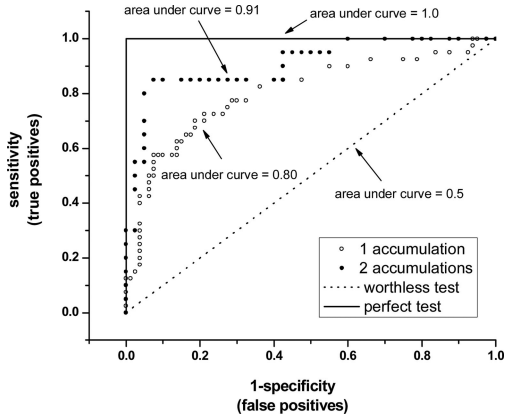

Fig. 7. ROC curve for one accumulation and two accumulation LIBS measurements on the 0 ppm sample (specificity) and the 2 ppm Al-doped model tissue (sensitivity). The noise cutoff criterion used in each measurement is decreasing from left to right. Also shown are the theoretical extrema for such ROC curves: a worthless test and a perfect test. The area under the curve is the figure of merit for determining the quality of the diagnostic accuracy of the test.

sitivity of 1. That is, the cutoff had to be placed below the background of the empty spectrum to detect aluminum 100% of the time. Of course, with a cutoff at this level, the rate of false positives was also 100%, as indicated in Fig. 7.

Also shown in Fig. 7 are the two theoretical extremes for an ROC curve. The diagonal dotted line indicates a worthless test and possesses an area under the curve (AUC) of 0.5. This denotes a test that conveys no statistically significant result, as all increases in sensitivity are accompanied by corresponding decreases in specificity. The step-function solid-line curve indicates a perfect test, and possesses an AUC of 1.0. Such a test always possesses a sensitivity of 1, no matter what the specificity is. Real tests tend to fall between these two theoretical extrema. The areas under the experimental LIBS curves were computed numerically using the MATLAB trapezoidal rule integration routine. The one accumulation ROC curve possessed an AUC of 0.80, while the two accumulation ROC curve possessed an AUC of 0.91. A rough guide for evaluating the accuracy of a diagnostic test such as this rates any ROC curve with an AUC from 0.90 to 1.0 as excellent, while an AUC from 0.50 to 0.60 rates as fairly worthless. The ROC curve constructed from the two accumulation LIBS analysis, with an AUC of 0.91, indicates the relative quality of this type of LIBS measurement for trace metal detection in soft tissues.

4. Conclusions

This paper has shown that LIBS can be a useful technology for detecting trace amounts of aluminum in a model tissue sample. Al can be detected to the sub-ppm level by observation of the Al resonance line at 396.1 nm after ablation with 80 mJ/pulse of 1064 nm laser radiation focused to a 1 mm $\times$ 0.1 mm spot with cylindrical optics. The Al line intensity was normalized by a nearby Ca II line at 393.366 nm to improve the reproducibility of the results, although unnormalized Al line intensities also effectively yielded the same sub-ppm LOD. The normalized Al emission line intensity was shown to be linear for Al concentrations ranging from 10 to 1140 ppm.

Additionally, a more realistic sampling methodology utilizing a limited number of laser pulses and spectral accumulations was investigated. A significant increase in sensitivity from 55% to 80% was shown in 2 ppm model tissues using a 3σ detection criterion merely by increasing the number of accumulations from 1 to 2. ROC curves were constructed to evaluate the accuracy of the LIBS analysis of a 2 ppm model tissue as a function of the cutoff criterion for aluminum detection. The single accumulation analysis yielded an area under the curve of 0.80, while the two accumulation analysis yielded an area of 0.91. This area is an appropriate figure of merit for such diagnostic tests, and indicates that the two accumulation LIBS analysis is an excellent detection technique for such tissues. Much more work needs to be done before this technique could be performed *in vivo*. We are currently investigating an all-optical-fiber delivery and light collection analysis that would allow a more realistic testing/sampling geometry. As well, experiments will need to be performed on real soft tissues contaminated with Al to determine the true ablation and detection efficiency. Nonetheless, as had been earlier reported by Kumar *et al.* [7], LIBS shows a great potential for development as an *in vivo* diagnostic tool for a variety of biomedical applications.

References

1. Wayne State University, Smart Sensors and Integrated Microsystems, "Neurological Implants," http://www.ssim.eng.wayne.edu/index.asp.
2. T. L. Walraven, R. Iezzi, J. P. McAllister, G. Auner, R. Givens, and G. Abrams, "Biocompatibility of a neurotransmitter based retinal and cortical visual prosthesis," Invest. Ophthalmol. Visual Sci. **43** (Suppl. 2), 4453 (2002).
3. C. A. Jaboro, A. R. Safadi, A. L. Lagman, R. Naik, V. Naik, G. W. Abrams, R. Iezzi, P. McAllister, and G. W. Auner, "A biocompatible study of chronic implants for electrical stimulation and chemical drug delivery to vision," Invest. Ophthalmol. Visual Sci. **43** (Suppl. 2), 4476 (2002).
4. R. Iezzi, N. P. Cottaris, S. D. Elfar, T. L. Walraven, T. M. Raza, R. Moncrieff, J. P. McAllister, G. W. Auner, R. R. Johnson, and G. W. Abrams, "Neurotransmitter-based retinal prosthesis modulation of retinal ganglion cell responses *in vivo,*" Invest. Ophthalmol. Visual Sci. **44** (Suppl. 2), 5083 (2003).
5. T. M. Raza, R. Iezzi, G. W. Auner, P. Siy, J. P. McAllister, N. P. Cottaris, S. D. Elfar, and G. W. Abrams, "Design of a high-channel-count current source for use in retinal and cortical visual prostheses," Invest. Ophthalmol. Visual Sci. **44** (Suppl. 2), 5086 (2003).
6. J. P. McAllister, J. Li, K. Deren, P. G. Finlayson, C. Jaboro, G. W. Auner, R. Baird, A. Lagman, R. Iezzi, and G. W. Abrams, "Chronic *in vivo* biocompatibility testing of materials used for visual prostheses," Invest. Ophthalmol. Visual Sci. **45** (Suppl. 2), 4214 (2004).
7. A. Kumar, F.-Y. Yueh, J. P. Singh, and S. Burgess, "Characterization of malignant tissue cells by laser-induced breakdown spectroscopy," Appl. Opt. **43,** 5399–5403 (2004).
8. O. Samek, D. C. S. Beddows, H. H. Telle, J. Kaiser, M. Liska, J. O. Caceres, and A. Gonzales Urena, "Quantitative laser-induced breakdown spectroscopy analysis of calcified tissue samples," Spectrochim. Acta Part B **56,** 865–875 (2001).
9. R. L. Vander Wal, T. M. Ticich, J. R. West, and P. A. Householder, "Trace metal detection by laser-induced breakdown spectroscopy," Appl. Spectrosc. **53,** 1226–1236 (1999).
10. C. M. John and R. W. Odom, "Static secondary ion mass spectrometry (SSIMS) of biological compounds in tissue and tissue-like matrices," Int. J. Mass Spectrom. Ion Processes **161,** 47–67 (1997).
11. B. MacMillan, B. Burke, B. Balcom, and G. Ziegler, "Phantom materials for single point imaging pulse sequences," Solid State Nucl. Magn. Reson. **28,** 106–110 (2005).
12. H. Kato, M. Kuroda, K. Yoshimura, A. Yoshida, K. Hanamoto, S. Kawasaki, K. Shibuya, and S. Kanazawa, "Composition of MRI phantom equivalent to human tissues," Med. Phys. **32,** 3199–3208 (2005).
13. Q. Chen, B. Suki, and K.-N. An, "Dynamic mechanical properties of agarose gels modeled by a fractional derivative model," Trans. ASME **126,** 666–671 (2004).
14. M. P. Mateo, L. M. Cabalin, J. M. Baena, and J. J. Laserna, "Surface interaction and chemical imaging in plasma spectrometry induced with a line-focused laser beam," Spectrochim. Acta Part B **57,** 601–608 (2002).
15. M. Adamson, A. Padmanabhan, G. J. Godfrey, and S. J.

Rehse are preparing a manuscript called "Broadband laser-induced breakdown spectroscopy at a water–gas interface: a study of bath gas-dependent molecular species."
16. S. Koch, W. Garen, M. Müller, and W. Neu, "Detection of chromium in liquids by laser induced breakdown spectroscopy (LIBS)," Appl. Phys. A **79,** 1071–1073 (2004).
17. A. Kumar, F. Y. Yueh, T. Miller, and J. Singh, "Detection of trace elements in liquids by laser-induced breakdown spectroscopy with a Meinhard nebulizer," Appl. Opt. **40,** 6040–6046 (2003).
18. J. Ingle, Jr., and S. Crouch, *Spectrochemical Analysis* (Prentice Hall, 1988).
19. S. J. Mason and N. E. Graham, "Areas beneath the relative operating characteristics (ROC) and relative operating levels (ROL) curves: statistical significance and interpretation," Q. J. R. Meteorol. Soc. **128,** 2145–2166 (2002).